STRUCTURAL CHEMISTRY

ISSN 2053-2296

An energetic study of differences in crystallization of *N*-(furan-3-yl)benzamide and *N*-(thiophen-3-yl)-benzamide

Wayne H. Pearson,*‡ Joseph J. Urban, Amy H. Roy MacArthur, Shirley Lin and Megan Mohadjer Beromi

Chemistry Department, United States Naval Academy, 572 Holloway Rd, Annapolis, MD 21402, USA. *Correspondence e-mail: waynehp21662@gmail.com

Received 15 June 2025
Accepted 31 July 2025

Edited by A. Lemmerer, University of the Witwatersrand, South Africa

‡ Retired

Keywords: crystal structure; disorder; molecular interaction energies; Hirshfeld surfaces; DFT calculations; energetic study; benzamide.

CCDC references: 2477643; 2477642

Supporting information: this article has supporting information at journals.iucr.org/c

The crystal structures of *N*-(furan-3-yl)benzamide, $C_{11}H_9NOS$, **FAP**, and *N*-(thiophen-3-yl)benzamide, $C_{11}H_9NO_2$, **TAP**, were determined by single-crystal X-ray diffraction at 173 K. The molecular units in both structures consist of three planar regions: a five-membered aryl ring, an amide linkage, and a phenyl ring. Both compounds crystallize in the space group $P\overline{1}$ with no solvent in the unit cell. There are two crystallographically unique, but geometrically similar, molecules in the asymmetric unit of **FAP**. N—H···O hydrogen bonds in **FAP** link the molecules into a linear chain lying along the *b* axis. The asymmetric unit in **TAP** is a disordered molecule containing contributions from two conformers with different orientations of the thiophenyl ring. N—H···O hydrogen bonds in **TAP** link the molecules into a linear chain lying along the *a* axis. Conformations of the gas-phase isolated conformers were predicted with density functional theory (DFT) calculations at the M06-2X/6-31+G(d) level. The conformers in **FAP** possess similar twist angles with respect to their calculated isolated conformers. However, the DFT calculations revealed a significant difference (>20°) in the twist angles of the thiophenyl rings–amide plane in **TAP** relative to the predicted gas-phase conformations. The π-stacking ring interactions between hydrogen-bonded molecules in the two crystal structures are not the same and are related to the difference in the magnitude of the dispersion and electrostatic interactions in the **FAP** and **TAP** environments.

1. Introduction

A series of arylamides was synthesized and isolated during the development of a microwave-assisted copper-catalyzed concurrent tandem catalytic methodology for the amidation of aryl chlorides and aryl bromides. Crystal structures for two of these arylamides have been published previously (Pearson *et al.*, 2022). The current work is a continuation of our investigation of the conformations of arylamides in the crystalline state *versus* the conformations of the isolated molecules as predicted by density functional theory (DFT) calculations. Analysis of the molecular interaction energies in the crystalline environments was performed to explain differences in the crystal packing. Our approach of comparing the conformational preferences of molecules in isolation to the observed conformations in the crystal state for these small molecules has the potential to yield insights about crystal packing in larger amide-containing systems of relevance in biological or materials chemistry.

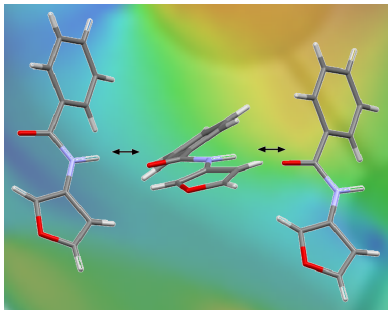

2. Synthesis and crystallization

Details of the syntheses of the title compounds **TAP** and **FAP** (Scheme 1) can be found in Chang *et al.* (2019) for *N*-(furan-3-

yl)benzamide and in Wood *et al.* (2022) for *N*-(thiophen-3-yl)-benzamide. Crystals for the compounds were grown by slow diffusion of hexanes into concentrated solutions of the amides in ethyl acetate. Melting points were determined to be 146–148 °C for **FAP** and 153–154 °C for **TAP**. Literature values of 145–147.3 °C for **FAP** and 154–155 °C for **TAP** were reported in Yasuhisa *et al.* (2017).

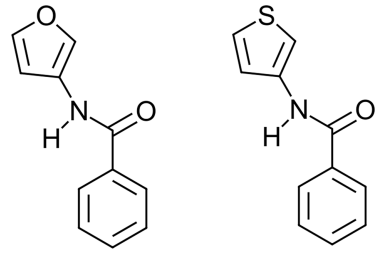

Scheme 1

3. Database survey

The Cambridge Structural Database (CSD, Version of April 2025, updated February 2025; Groom *et al.*, 2016) was searched for possible crystal structures of these compounds. No entries were found.

4. X-ray refinement

Ellipsoidal plots of the molecules in the asymmetric units of **FAP** and **TAP** are shown in Figs. 1 (**FXA** and **FXB**) and 2 (**TXA** and **TXB**).

Refinement for **FAP** resulted in $R1$ = 0.058 for all data. Initial refinements for **TAP** converged to $R1$ = 0.118, with indications of a disordered thiophenyl ring in the asymmetric unit. The disorder is the result of two different conformers occupying the molecular sites, with orientations of the thiophenyl rings differing by ∼180° (179.87°). A similar type of disorder was found in the crystal structure of *N*′-[(*E*)-pyridin-2-ylmethylidene]-2-(thiophen-2-yl)ethanohydrazide (Garbutt *et al.*, 2022). For **TAP**, conformers **TXA** [Fig. 2(*a*)] and **TXB** [Fig. 2(*b*)] are components of the disordered asymmetric unit. It was decided to use the simplest possible model involving split atoms for C10 and S1. Incorporation of disorder into the **TAP** model resulted in $R1$ = 0.044 for all data. Occupancies of the two conformers refined to 0.702 (2) for **TXA** and 0.298 (2) for **TXB**. The nature of the disorder and the small amount of electron density associated with the C atoms of conformer **B** required employing distance restraints and atomic displacement parameter constraints to the disordered atoms. Please see the supporting information for full details.

Difference density maps revealed the presence of H-atom electron densities that could be modeled using unrestrained C—H bond lengths and isotropic displacement parameters. Unrestrained N—H distances refined to very short bonds of approximately 0.85 Å. As a result, the N—H bond lengths in the hydrogen-bonded interactions were refined with a distance restraint of 1.00 Å. This restraint is consistent with the results of the DFT and Molecular energy interaction (MEI) calculations. The H atom associated with the minor component of disorder in **TAP** (H10*B*) could not be treated with a direct refinement and was modeled using a riding model. Details of the refinement choices can be found in the supporting information.

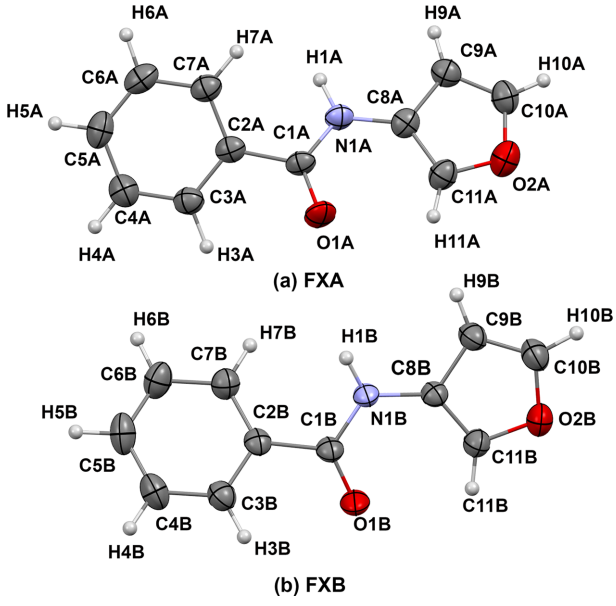

Figure 1
Displacement ellipsoid plots (50% probability level) of the two independent molecules in the asymmetric unit in **FAP**, showing (*a*) **FXA** and (*b*) **FXB**.

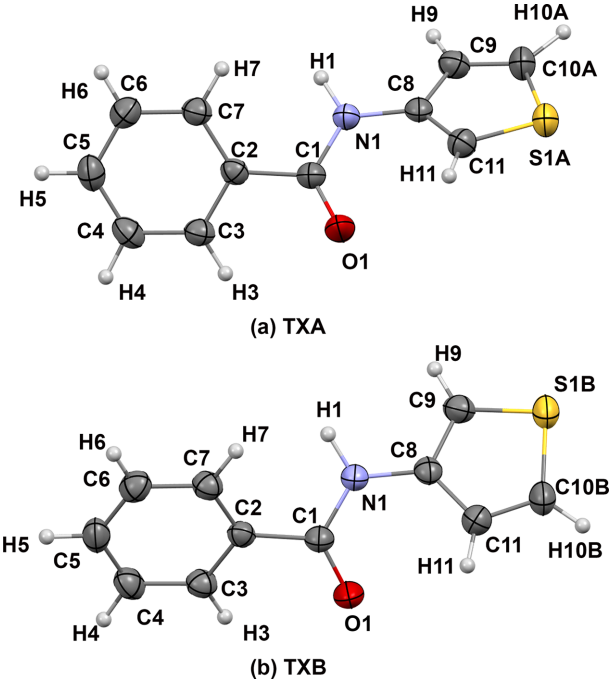

Figure 2
Displacement ellipsoid plots (50% probability level) of the two conformers in the disordered asymmetric unit in **TAP**, showing (*a*) **TXA** and (*b*) **TXB**.

Table 1
Experimental details.

	TAP	**FAP**
Crystal data		
Chemical formula	$C_{11}H_9NOS$	$C_{11}H_9NO_2$
M_r	203.25	187.19
Crystal system, space group	Triclinic, $P\overline{1}$	Triclinic, $P\overline{1}$
Temperature (K)	173	172
a, b, c (Å)	5.2909 (4), 7.6252 (5), 12.1529 (8)	9.0111 (3), 9.8038 (3), 11.3362 (4)
α, β, γ (°)	83.865 (2), 78.470 (2), 88.762 (2)	109.081 (3), 99.580 (3), 90.499 (3)
V (Å^3)	477.65 (6)	931.11 (6)
Z	2	4
Radiation type	Mo $K\alpha$	Mo $K\alpha$
μ (mm^{-1})	0.30	0.09
Crystal size (mm)	0.41 × 0.23 × 0.11	0.28 × 0.24 × 0.16
Data collection		
Diffractometer	Bruker SMART APEX II CCD	Rigaku OD SuperNova Dual source diffractometer with an Atlas detector
Absorption correction	Multi-scan (*SADABS*; Bruker, 2018)	Gaussian (*CrysAlis PRO*; Rigaku OD, 2020)
T_{min}, T_{max}	0.741, 1.000	0.589, 1.000
No. of measured, independent and observed [$I > 2\sigma(I)$] reflections	13278, 1970, 1674	21889, 4363, 3580
R_{int}	0.057	0.027
$(\sin\theta/\lambda)_{max}$ (Å^{-1})	0.626	0.653
Refinement		
$R[F^2 > 2\sigma(F^2)]$, $wR(F^2)$, S	0.042, 0.115, 1.05	0.047, 0.125, 1.09
No. of reflections	1970	4363
No. of parameters	167	325
No. of restraints	7	2
H-atom treatment	H atoms treated by a mixture of independent and constrained refinement	All H-atom parameters refined
$\Delta\rho_{max}$, $\Delta\rho_{min}$ (e Å^{-3})	0.30, −0.28	0.43, −0.21

Computer programs: *APEX3* (Bruker, 2018), *CrysAlis PRO* (Rigaku OD, 2020), *SHELXT2014* (Sheldrick, 2015*a*), *WinGX* (Farrugia, 2012), *SHELXL2018* (Sheldrick, 2015*b*), *Mercury* (Macrae *et al.*, 2020), *CrystalExplorer* (Spackman *et al.*, 2021), and *publCIF* (Westrip, 2010).

Crystal data, data collection and structure refinement details are summarized in Table 1.

5. Features of the FAP and TAP crystal structures

The unit cells for **FAP** and **TAP** are shown in Fig. 3. Hydrogen bonding is present between molecules in both crystals forming linear chains along the *b* axis in **FAP** and along the *a* axis in **TAP**. The hydrogen-bond geometries are listed in Tables 2 and 3.

An important aspect of the geometries of the conformers in each unit cell is the relationship between the chalcogen atoms (O and S) in the amide plane and the five-membered ring. *Syn* conformers have the chalcogen atoms on the same side of the molecule, while *anti* conformers have the chalcogen atoms on opposite sides of the molecule. The unit cell in **FAP** [Fig. 3(*a*)] contains only *syn* conformers (**FXA and FXB**) and inverted forms. Fig. 3(*b*) represents the disordered structure of **TAP**. The disorder in **TAP** is a result of the ability of both *syn* and *anti* conformers (**TXA** and **TXB**) to occupy the same crystallographic site in different unit cells.

The bond lengths and angles in these four conformers are typical of those in small organic molecules. Experimental bond lengths and angles are contained in the supporting information.

Twist angles between the the aryl regions of the conformers show similarities and variations in **FAP** and **TAP**. Phenyl–amide twist angles range from 26.0 (2) to 30.3 (1)° in both compounds. **FAP** conformers **FXA** and **FXB** exhibit relatively minor twist angles of 1.6 (2)–6.8 (2)° between the amide plane and the furanyl ring. **TAP** conformers **TXA** and **TXB** have fairly large twist angles of 31.1 (1) and 31.0 (2)° between the amide plane and the thiophenyl ring.

6. DFT calculations on molecules in isolation

Quantum-chemical DFT calculations were performed to find the conformations of global minimum energy for the conformers of the two compounds in isolation. Calculations were performed with the *GAUSSIAN16* (Frisch *et al.*, 2016)

Table 2
Hydrogen-bond geometry (Å, °) for **FAP**.

D—H···A	D—H	H···A	D···A	D—H···A
N1B—H1B···O1A	0.94 (2)	1.96 (2)	2.8234 (17)	151 (2)
N1A—H1A···O1B^{i}	0.97 (2)	1.91 (2)	2.8374 (18)	159 (2)

Symmetry code: (i) $x, y-1, z$.

Table 3
Hydrogen-bond geometry (Å, °) for **TAP**.

D—H···A	D—H	H···A	D···A	D—H···A
N1—H1···O1^{i}	0.97 (1)	2.17 (1)	3.078 (2)	154 (2)

Symmetry code: (i) $x+1, y, z$.

program suite on Department of Defense High Performance Modernization resources. Initial conformer searching was performed at the molecular mechanics level with the MMFF force field as implemented in *Spartan'14* molecular modeling software (Wavefunction Inc., 2014). Viable structures were then subjected to complete geometry optimizations in *GAUSSIAN16* at the M06-2X/6-31+G(d) level (Zhao & Truhlar, 2008). Frequency calculations were performed at M06-2X/6-31+G(d) to confirm that all stationary points were minima. Calculations of Gibbs free energies at 298.15 K were performed using standard routines in *GAUSSIAN16*.

7. Comparison of conformers observed in the crystal state and conformers calculated with DFT for molecules in isolation

Comparison of the experimental and DFT-calculated conformers for **FAP** and **TAP** are shown in Fig. 4. The experimental conformers in **FAP** and **TAP** are labeled as **FXA**, **FXB**, **TXA**, and **TXB**. The corresponding isolated molecules, as determined by M06-2X/6-31+G(d) optimization, are labeled **FDA**, **FDB**, **TDA**, and **TDB**.

FDA and **FDB** are isoergic conformers. Conformer **FDANTI** has no analog in **FAP** but corresponds to the minimum energy for possible *anti* conformers of the isolated furanyl compound. **FDA** and **FDB** are 7.66 kJ mol^{-1} lower in internal energy than conformer **FDANTI**. The **FDA** and **FDB** isomers have calculated Gibbs free energies that are 5.94 kJ mol^{-1} lower than **FDANTI**. Mole fractions, based upon this free energy difference, would be 0.90 for the *syn* conformers *versus* 0.10 for the *anti* conformer. **TDA** is the result of M06-2X/6-31+G(d) energy minimization of the *syn* conformer **TXA. TDB** is the result of M06-2X/6-31+G(d) energy minimization of the *anti* conformer **TXB. TDA** has an internal energy 4.98 kJ mol^{-1} lower than **TDB**. After conversion to free energy, **TDA** is found to be 3.43 kJ mol^{-1} lower in Gibbs free energy than **TDB**. This ΔG value corresponds to mole fractions of 0.80 for **TDA** and 0.20 for **TDB**, similar to the refined occupancies for **TXA** (0.70) and **TXB** (0.30).

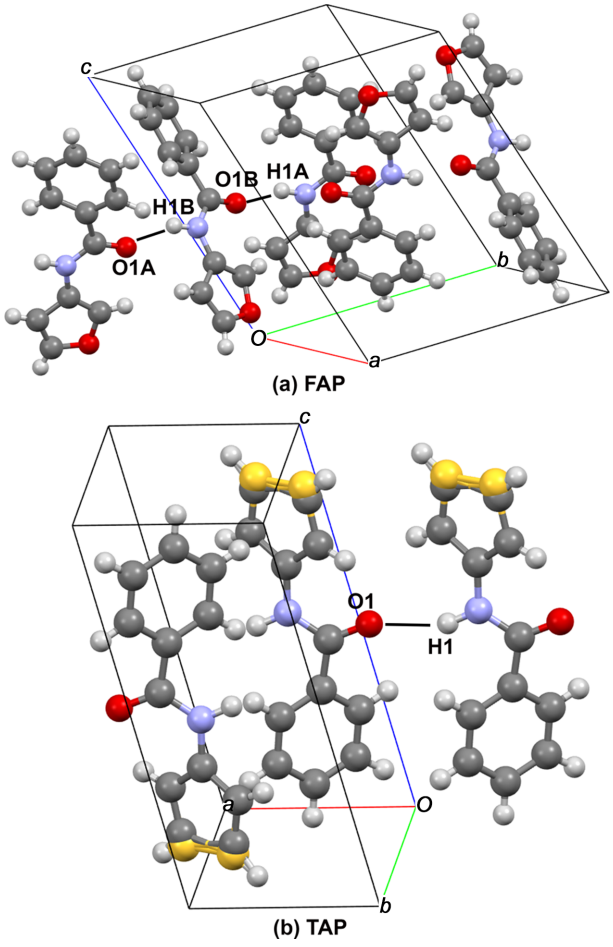

Figure 3
The unit cells of (*a*) **FAP** and (*b*) **TAP**. Hydrogen bonds are shown as black lines.

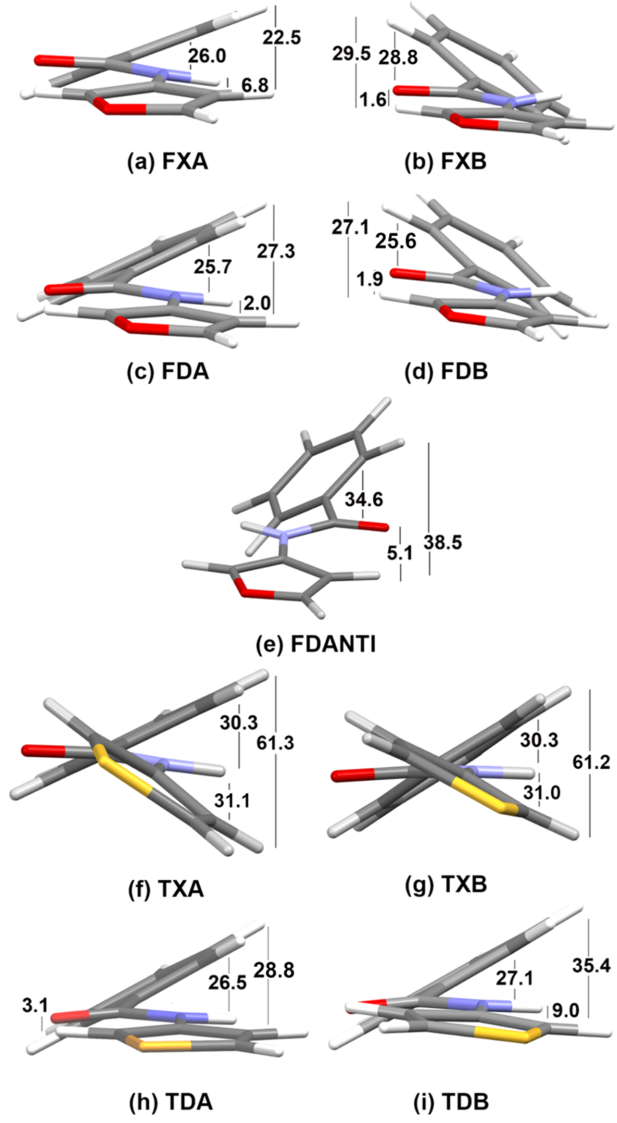

Figure 4
Experimental and DFT conformers in **FAP** and **TAP**. The angles between planar regions are given in degrees (°).

Table 4
Angles (°) between least-squares planes.

Calculations performed in *Mercury* (Macrae *et al.*, 2020).

Conformer	Phenyl–amide	Amide–heterocycle	Phenyl–heterocycle
FXA	26.0 (2)	6.8 (2)	22.5 (1)
FXB	28.8 (2)	1.6 (2)	29.5 (1)
FDA	25.7	2.0	27.3
FDB	25.6	1.9	27.1
FDANTI	34.6	5.1	38.5
TXA	30.3 (1)	31.1 (1)	61.3 (1)
TXB	30.3 (1)	31.0 (2)	61.2 (2)
TDA	26.5	3.1	28.8
TDB	27.1	9.0	35.4

Twist angles between the planar regions in the conformers are listed in Table 4 and shown in Fig. 4. A major difference between the conformers in **FAP** and **TAP** involves the twist angles between the five-membered aromatic rings and the amide plane. The experimental furanyl–amide plane twist angles in the **FXA** and **FXB** conformers differ from the corresponding angles in **FDA** and **FDB** by no more than 5°. The thiophenyl–amide plane angles in **TXA** and **TXB** are in excess of 20° greater than the corresponding angles in **TDA** and **TDB**. These twist angles will be discussed further in Section 10.

The decision for modeling the H-atom positions without using a riding model was guided, in part, by examination of the M06-2X/6-31+G(d) results. The results for **FDA**, **FDB**, **TDA**, and **TDB** (shown in the supporting information) predict that the C—H bonds do not bisect the interior ring angles of the five-membered rings. Using a riding model in the refinements of **FAP** and **TAP** would force the corresponding H atoms in **FXA**, **FXB**, **TXA**, and **TXB** to bisect the interior ring angles of the five-membered rings. A literature search of recent crystal structures containing furanyl and thiophenyl rings resulted in one report (Majer *et al.*, 2020) of refined H-atom positions in a furanyl ring. In that study, the C—H bonds do not bisect the interior ring angles. Comparisons of the refined C—H terminal angles in the furanyl rings of **FXA** and **FXB** with those in **FDA** and **FDB** and the Majer study are shown in Fig. 5. The results indicate that the experimental H-atom positions in **FAP** and **TAP** should be refined and not fixed with a riding model.

Direct refinement of H-atom positions results in some differences in the terminal phenyl ring angles when compared to the M06-2X/6-31+G(d) results. Further discussion of this finding can be found in Section 9. A full comparison of bond lengths and angles in the X-ray models and M06-2X/6-31+G(d) calculations can be found in the supporting information.

8. Why is FAP an ordered structure while TAP is disordered?

The reason for an ordered structure in **FAP** *versus* a disordered structure in **TAP** appears to involve the nature of the conformers that are present in the unit cells. The results of the *syn*/*anti* population analyses from the M06-2X/6-31+G(d) results (**FDA**/**FDANTI** 0.90/0.10 and **TDA**/**TDB** 0.80/0.20) indicate that if *anti* conformers were to exist in the crystals, they would need to adapt to an environment that is largely determined by the *syn* conformers. Disorder in **TAP** is a reasonable result based upon the structural similarity of the *syn* and *anti* conformers. The thiophenyl rings differ by approximately 180° between the *syn* and *anti* conformers in both experimental and calculated conformers, while the phenyl–amide twist angles remain relatively unchanged. For the **FAP** conformers shown in Fig. 4, the amide–phenyl plane angle in **FDANTI** (34.6°) is larger than the amide–phenyl plane angles in the calculated and experimentally observed *syn* conformers **FDA** (25.7°), **FDB** (25.6°), **FXA** (26.0°), and **FXB** (28.8°). In order to occupy the equivalent crystallographic sites as the *syn* conformers in **FAP**, the amide–phenyl twist angle in **FDANTI** would have to decrease on the order of 6–9°. This amount of twist is much larger than the modest amide–phenyl twist angle differences between the **FX** and **FD** *syn* conformers of no more than 3°. Rather than accommodate this 6–9° twisting of the amide–phenyl angle, the *syn* conformers in **FAP** appear to prefer to be in an ordered crystal environment with the exclusion of the *anti* conformers.

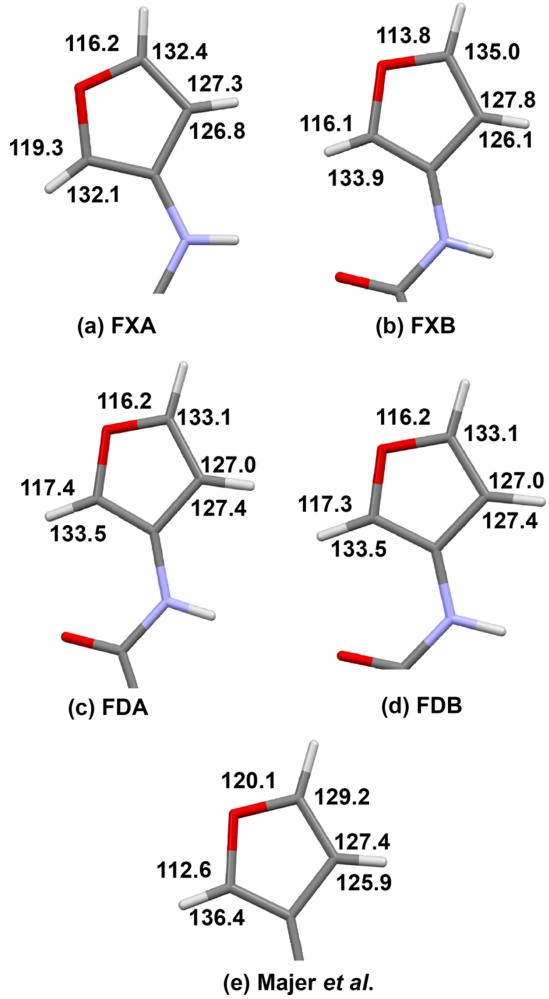

Figure 5
C—H terminal angles (in °) for the furanyl ring in (*a*) **FXA**, (*b*) **FXB**, (*c*) **FDA**, (*d*) **FDB**, and (*e*) Majer *et al.* (2020).

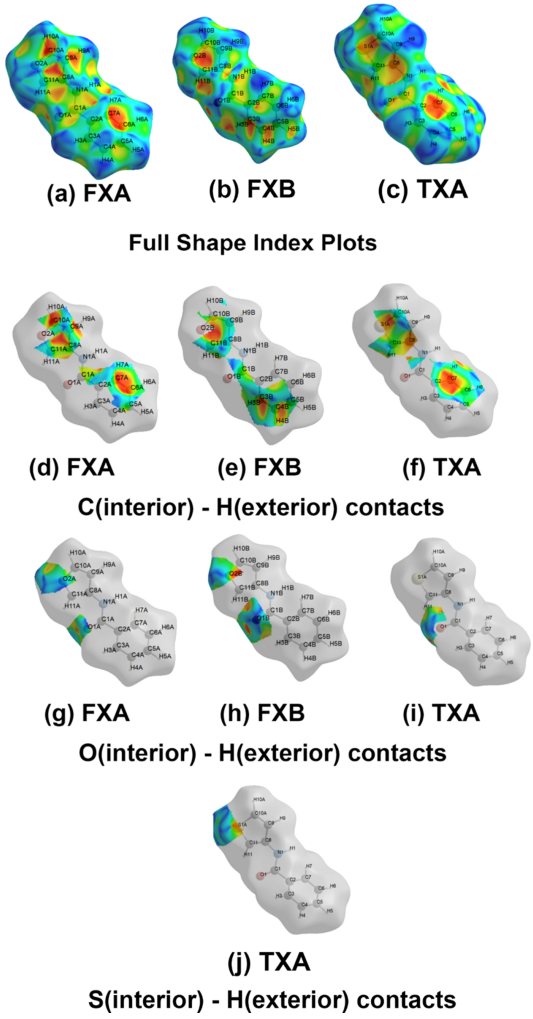

Figure 6
The Hirshfeld surfaces, with shape index plots.

9. Hirshfeld surfaces and close contacts

Hirshfeld surfaces were calculated using *CrystalExplorer* (Version 21.5; Spackman *et al.*, 2021). Fig. 6 contains views of the Hirshfeld surfaces with shape index plots for **FXA**, **FXB**, and **TXA**. It is not possible to develop a Hirshfeld surface for **TAP** using the disordered crystalline environment. As the nearest approximation, a Hirshfeld surface was developed for **TXA** using a hypothetical crystal environment that was only composed of the major conformer **TXA**. The shape index plots show the presence of closest contacts as the red indentations in the surface function. Fig. 6 contains isolated views of external hydrogen contacts with internal C, S, and O atoms. Hydrogen bonding, electrophilic association with the ring O and S atoms, and π-stacking contacts are revealed in these surface plots. Fingerprint plots for C···H/H···C contacts involving both internal and external H atoms are shown in Fig. 7 for **FXA**, **FXB**, and **TXA**. These plots reveal that the packing of these contacts around **TXA** (35.7%) occupies a larger relative area than in **FXA** (27.4%) and **FXB** (28.9%). These close H-atom contacts may be a part of the explanation for the C—H bonds in the experimental phenyl rings having angular deviations from the values predicted by M06-2X/6-31 +G(d) calculations on the isolated molecules. Three-dimensional videos and additional fingerprint plots for these Hirshfeld surfaces can be found in the supporting information.

10. Molecular interaction energy (MIE) analysis in FAP and TAP

In order to find the underlying reasons for the difference in the five-membered ring–amide plane orientations in **FAP** and **TAP**, we investigated the energetics of the packing of the conformers in both crystal structures.

Images of the nearest-neighbor environments are shown in Figs. 8(*a*)–(*f*). The molecules are color-coded with respect to molecular interaction energy (MIE) with the central molecule. The interaction energies were calculated using *Tonto* (Jayatilaka & Grimwood, 2003) using the CE-B3LYP/6-31G(d,p) modeling in *CrystalExplorer* (Spackman *et al.*, 2021). The MIE values are very similar in both crystals, with average values of −38 (7) kJ mol^{-1} for **FAP** and −35 (8) kJ mol^{-1} for **TAP**. For **TAP**, Figs. 8(*c*)–(*f*) show MIEs for central **TXA** or **TXB** molecules surrounded by hypothetical homogeneous environments composed of either **TXA** or **TXB** conformers. Fig. 8(*g*) summarizes the results for E_{tot} values included in Figs. 8(*c*)–(*f*). These results demonstrate no significant energy differences for conformer interactions of type **A**–**A**, **B**–**B**, or **A**–**B**. Videos with three-dimensional views of the MIEs can be found in the supporting information.

There is a significant difference in the π-stacking of aryl rings involved in the hydrogen-bonded molecules. Hydrogen bonds were revealed using *SHELXL* (Sheldrick, 2015*b*) and verified using *PLATON* (Spek, 2020). The hydrogen-bond interactions in **FAP** and **TAP** are highlighted in Figs. 9(*a*) and 9(*b*). The numbers assigned to molecules are the same as used in Fig. 8. In **FAP**, the furanyl–furanyl planar interactions of the central molecule to molecules 1 and 3 are T-shaped with an angle of 57.8 (2)°. In **TAP**, the thiophenyl–thiophenyl interactions of the central molecule to molecules 1 and 4 are parallel-displaced. The MIE values, shown in Fig. 8 and referenced in Fig. 9, reveal a larger electrostatic interaction between molecules with hydrogen bonding in **FAP**, while larger dispersion interactions exist between the hydrogen-bonded molecules in **TAP**. This observation is consistent with T-shaped π-stacking being driven by electrostatic interactions, while parallel displacement interactions are driven more by

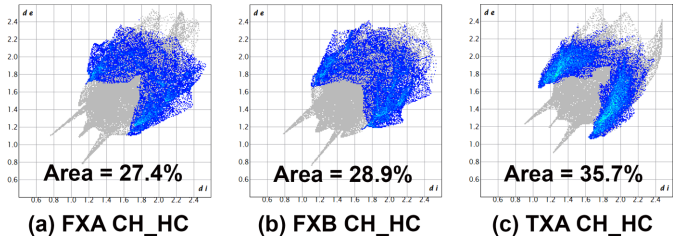

Figure 7
Fingerprint plots for C···H/H···C close contacts around (*a*) **FXA**, (*b*) **FXB**, and (*c*) **TXA**.

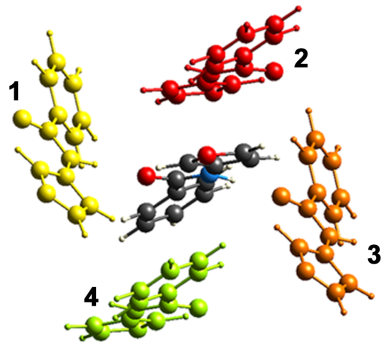

Position	R	E_ele	E_pol	E_dis	E_rep	E_tot
FXA_1	4.95	-42.4	-7.4	-22.7	30.4	-42
FXA_2	4.33	-16.6	-2.1	-38.6	16.0	-41
FXA_3	4.86	-44.8	-7.6	-24.3	31.5	-45
FXA_4	4.68	-4.5	-1.0	-33.6	12.1	-27

(*a*)

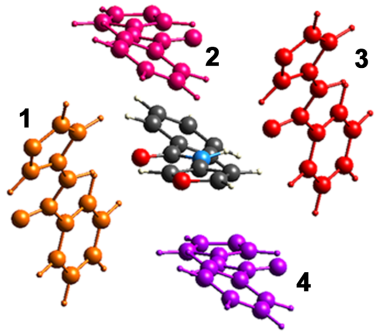

Position	R	E_ele	E_pol	E_dis	E_rep	E_tot
FXB_1	4.86	-44.8	-7.6	-24.3	31.5	-45
FXB_2	4.41	-5.9	-1.2	-32.7	11.1	-29
FXB_3	4.95	-42.4	-7.4	-22.7	30.4	-42
FXB_4	4.64	-14.1	-1.7	-31.7	12.2	-35

(*b*)

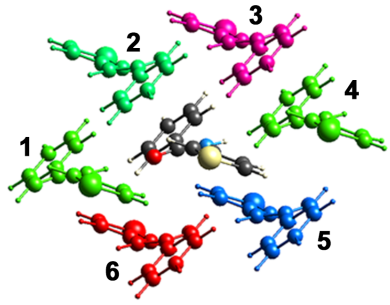

Position	R	E_ele	E_pol	E_dis	E_rep	E_tot
TXAA_1	5.29	-35.8	-5.6	-28.6	23.5	-46
TXAA_2	4.43	-11.9	-1.4	-32.8	14.5	-32
TXAA_3	5.02	-14.6	-1.9	-31.7	18.8	-29
TXAA_4	5.29	-35.8	-5.6	-28.6	23.5	-46
TXAA_5	5.03	-7.2	-1.3	-26.7	10.9	-24
TXAA_6	4.64	-10.3	-2.2	-34.6	15.4	-32

(*c*)

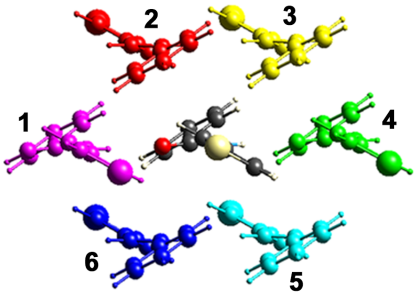

Position	R	E_ele	E_pol	E_dis	E_rep	E_tot
TXAB_1	4.64	-35.8	-5.6	-28.6	24.2	-46
TXAB_2	5.41	-11.2	-1.5	-33.1	14.3	-31
TXAB_3	5.17	-13.2	-1.8	-31.8	17.7	-29
TXAB_4	4.9	-34.7	-5.7	-28.7	22.7	-46
TXAB_5	4.55	-8.1	-1.4	-26.6	11.3	-25
TXAB_6	5	-11.5	-2.1	-34.6	16.8	-31

(*d*)

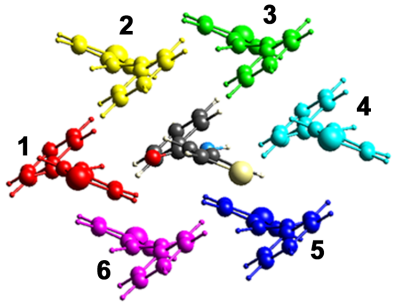

Position	R	E_ele	E_pol	E_dis	E_rep	E_tot
TXBA_1	5.41	-34.7	-5.7	-28.7	22.7	-46
TXBA_2	4.55	-11.2	-1.5	-33.1	14.3	-31
TXBA_3	5	-13.2	-1.8	-31.8	17.7	-29
TXBA_4	5.17	-35.8	-5.6	-28.6	24.2	-46
TXBA_5	4.9	-8.1	-1.4	-26.7	11.3	-25
TXBA_6	4.64	-11.5	-2.1	-34.6	16.8	-31

(*e*)

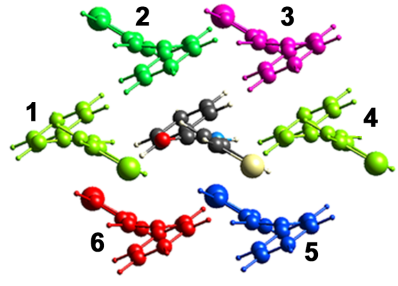

Position	R	E_ele	E_pol	E_dis	E_rep	E_tot
TXBB_1	5.29	-35.8	-5.7	-28.7	23.5	-47
TXBB_2	4.67	-10.5	-1.6	-33.3	14.2	-31
TXBB_3	4.98	-11.8	-1.6	-32.0	16.5	-29
TXBB_4	5.29	-35.8	-5.7	-28.7	23.5	-47
TXBB_5	4.77	-9.2	-1.5	-26.5	11.6	-26
TXBB_6	4.64	-12.8	-2.0	-34.7	18.2	-31

(*f*)

E_tot at Position	TXAA	TXAB	TXBA	TXBB
1	-46.5	-45.9	-46.3	-46.7
2	-31.7	-31.4	-31.4	-31.1
3	-29.3	-29.1	-29.1	-28.9
4	-46.5	-46.3	-45.9	-46.7
5	-24.3	-24.8	-24.9	-25.5
6	-31.7	-31.4	-31.4	-31.2

(*g*)

Figure 8
Results of MIE calculations (kJ mol^{-1}) for nearest-neighbor packing around (*a*) **FXA**, (*b*) **FXB**, (*c*) **TXA** surrounded by **A** conformers, (*d*) **TXA** surrounded by **B** conformers, (*e*) **TXB** surrounded by **A** conformers and (*f*) **TXB** surrounded by **B** conformers. *R* is the separation of molecular centroids in Ångstroms. E_{tot} (total interaction energy) is the sum of E_{ele} (electrostatic), E_{pol} (polarization), E_{dis} (dispersion) and E_{rep} (repulsion) terms. Fig. 8(*g*) contains the summary of E_{tot} values in Figs. 8(*c*)–(*f*).

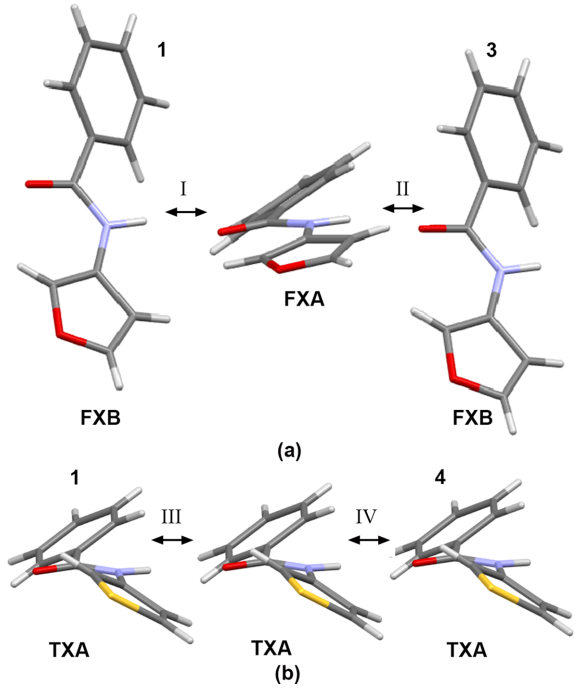

Figure 9
Electrostatic and dispersion contributions (kJ mol^{-1}) to the interaction energies for hydrogen-bonded molecules in (*a*) **FAP** and (*b*) **TAP**, with $E_{ele} = -42$ and $E_{dis} = -23$ for **I**, $E_{ele} = -45$ and $E_{dis} = -24$ for **II**, $E_{ele} = -36$ and $E_{dis} = -29$ for **III**, and $E_{ele} = -36$ and $E_{dis} = -29$ for **IV**. Approximate uncertainties are ±1 kJ mol^{-1}. The molecule numbering is the same as in Fig. 8.

dispersion (Banerjee *et al.*, 2019). It is expected that a ring containing an O atom (**FAP**) would tend towards harder electrostatic interactions, while a ring containing an S atom (**TAP**) would tend towards softer dispersive interactions. Rather than maintain a parallel orientation between aryl rings in hydrogen-bonded molecules similar to that in **TAP**, the two furanyl conformers rotate relative to each other to establish the asymmetric unit with T-shaped furanyl stacking. This arrangement of the hydrogen bond does not require significant tilting of the furanyl ring–amide plane within the **FAP** conformers. The tilting of the thiophenyl–amide plane in the asymmetric unit of **TAP** allows for the establishment of the hydrogen bond while developing a dispersive interaction between parallel π-clouds of thiophenyl rings in neighboring molecules. The difference in hydrogen-bonding modes is a significant feature that contributes to the difference in the crystal environments of **FAP** and **TAP**.

11. Summary

The investigation of the crystal packing in **FAP** and **TAP** has revealed similarities and differences in how these two very similar molecules, *N*-(furan-3-yl)benzamide and *N*-(thiophen-3-yl)benzamide, form crystalline states. While hydrogen bonding is present in both crystals, the orientations of the molecules in the hydrogen bonding is quite different. In **FAP**, the furanyl molecules exhibit intermolecular twists while maintaining molecular conformations that are very similar to those of the gas-phase molecules that were predicted by DFT optimization. In **TAP**, the thiophenyl molecules have amide–thiophenyl twist angles that differ in excess of 20° from the predicted gas-phase molecules. This degree of twisting allows the hydrogen bonding in **TAP** to form with parallel-displaced molecules. This difference in behavior is correlated with a larger electrostatic interaction energy between the molecules in **FAP** that favors the T-stacking of the furanyl rings. The disorder in **TAP** is the result of the similarities between the *syn* (**TXA**) and *anti* (**TXB**) conformers with coplanar thiophenyl and phenyl rings. These conformers occupy, at random, the same crystallographic site, while the molecular interaction energies between possible conformer pairs vary by less that 1 kJ mol^{-1}. A similar type of disorder involving conformers in **FAP** is less probable due to the increased phenyl–amide twist angle in the calculated gas-phase *anti* conformer **FDANTI** *versus* the *syn* conformers **FDA** or **FDB**.

Acknowledgements

The authors acknowledge Dr Chip Nataro of Lafayette College for performing the CSD search. The views expressed in this document are those of the authors and do not reflect the official policy or position of the U.S. Naval Academy, Department of the Navy, the Department of Defense, or the U.S. Government.

Funding information

Funding for this research was provided by: Department of Defense HPC Modernization Program (award to Joseph Urban); Office of Naval Research (award to Shirley Lin and Amy H. Roy MacArthur).

References

Banerjee, A., Saha, A. & Saha, B. K. (2019). *Cryst. Growth Des.* **19**, 2245–2252.
Bruker (2018). *APEX3*, *SAINT*, *SADABS*, and *SHELXTL*. Bruker AXS Inc, Madison, Wisconsin, USA.
Chang, R. K., Clairmont, B. P., Lin, S. & MacArthur, A. H. R. (2019). *Organometallics* **38**, 4448–4454.
Farrugia, L. J. (2012). *J. Appl. Cryst.* **45**, 849–854.
Frisch, M. J., Trucks, G. W., Schlegel, H. B., Scuseria, G. E., Robb, M. A., Cheeseman, J. R., Scalmani, G., Barone, V., Mennucci, B., Petersson, G. A., Nakatsuji, H., Caricato, M., Li, X., Hratchian, H. P., Izmaylov, A. F., Bloino, J., Zheng, G., Sonnenberg, J. L., Hada, M., Ehara, M., Toyota, K., Fukuda, R., Hasegawa, J., Ishida, M., Nakajima, T., Honda, Y., Kitao, O., Nakai, H., Vreven, T., Montgomery, J. A., Peralta, J. E., Ogliaro, F., Bearpark, M., Heyd, J. J., Brothers, E., Kudin, K. N., Staroverov, V. N., Kobayashi, R., Normand, J., Raghavachari, K., Rendell, A., Burant, J. C., Iyengar, S. S., Tomasi, J., Cossi, M., Rega, N., Millam, J. M., Klene, M., Know, J. E., Cross, J. B., Bakken, V., Adamo, C., Jaramillo, J., Gomperts, R., Stratmann, R. E., Yazyev, O. A., Austin, J., Cammi, R., Pomelli, C., Ochterski, J. O., Martin, R. L., Morokuma, K., Zakrzweski, V. G., Voth, G. A., Salvador, P., Dannenberg, J. J., Dapprich, S., Daniels, A. D., Farkas, O., Foresman, J. B., Ortiz, J. V., Cioslowski, J. & Fox, D. J. (2016). *GAUSSIAN16*. Revision C.01. Gaussian Inc., Wallingford, CT, USA. https://gaussian.com/.

Garbutt, J. L., da Costa, C. F., deSouza, M. V. N., Wardell, S. M. S. V., Wardell, J. L. & Harrison, W. T. A. (2022). *Acta Cryst.* E**78**, 619–624.
Groom, C. R., Bruno, I. J., Lightfoot, M. P. & Ward, S. C. (2016). *Acta Cryst.* B**72**, 171–179.
Jayatilaka, D. & Grimwood, D. J. (2003). *Tonto: a fortran based object-oriented system for quantum chemistry and crystallography*, in *Computational science – ICCS 2003. Lecture notes in computer science*, Vol. 2660, edited by P. M. A. Sloot, D. Abramson, A. V. Bogdanov, Y. E. Gorbachev, J. J. Dongarra & A. Y. Zomaya. Berlin, Heidelberg: Springer.
Macrae, C. F., Sovago, I., Cottrell, S. J., Galek, P. T. A., McCabe, P., Pidcock, E., Platings, M., Shields, G. P., Stevens, J. S., Towler, M. & Wood, P. A. (2020). *J. Appl. Cryst.* **53**, 226–235.
Majer, T., Schollmeyer, D., Koch, P. & Gross, H. (2020). *IUCRData* **5**, x201578.
Pearson, W. H., Urban, J. J., MacArthur, A. H. R., Lin, S. & Cabrera, D. W. L. (2022). *Acta Cryst.* E**78**, 297–305.
Rigaku OD (2020). *CrysAlis PRO*. Rigaku Oxford Diffraction Ltd, Yarnton, Oxfordshire, England.
Sheldrick, G. M. (2015*a*). *Acta Cryst.* A**71**, 3–8.
Sheldrick, G. M. (2015*b*). *Acta Cryst.* C**71**, 3–8.
Spackman, P. R., Turner, M. J., McKinnon, J. J., Wolff, S. K., Grimwood, D. J., Jayatilaka, D. & Spackman, M. A. (2021). *J. Appl. Cryst.* **54**, 1006–1011.
Spek, A. L. (2020). *Acta Cryst.* E**76**, 1–11.
Wavefunction Inc. (2014). *Spartan'14*. Version 6.1.8. Wavefunction Inc., Irvine, CA, USA. https://downloads.wavefun.com/Spartan14Manual.pdf.
Westrip, S. P. (2010). *J. Appl. Cryst.* **43**, 920–925.
Wood, H. J., Lin, S. & MacArthur, A. H. R. (2022). *Organometallics* **41**, 3109–3114.
Yasuhisa, T., Hirano, K. & Miura, M. (2017). *Chem. Lett.* **46**, 463–465.
Zhao, Y. & Truhlar, D. J. (2008). *Theor. Chem. Acc.* **120**, 215–241.

supporting information

Acta Cryst. (2025). C**81**, 539-547 [https://doi.org/10.1107/S2053229625006886]

An energetic study of differences in crystallization of *N*-(furan-3-yl)benzamide and *N*-(thiophen-3-yl)benzamide

Wayne H. Pearson, Joseph J. Urban, Amy H. Roy MacArthur, Shirley Lin and Megan Mohadjer Beromi

Computing details

N-(Thiophen-3-yl)benzamide (TAP)

Crystal data

$C_{11}H_9NOS$
$M_r = 203.25$
Triclinic, $P\overline{1}$
$a = 5.2909$ (4) Å
$b = 7.6252$ (5) Å
$c = 12.1529$ (8) Å
$\alpha = 83.865$ (2)°
$\beta = 78.470$ (2)°
$\gamma = 88.762$ (2)°
$V = 477.65$ (6) Å^3
$Z = 2$
$F(000) = 212$
$D_x = 1.413$ Mg m^{-3}
$D_m = 1.35$ (3) Mg m^{-3}
D_m measured by flotation in potassium carbonate solution
Melting point: 427 K
Mo $K\alpha$ radiation, $\lambda = 0.71073$ Å
Cell parameters from 6954 reflections
$\theta = 2.7$–26.4°
$\mu = 0.30$ mm^{-1}
$T = 173$ K
Parallelpiped, colourless
0.41 × 0.23 × 0.11 mm

Data collection

Bruker SMART APEX II CCD diffractometer
Radiation source: sealed X-ray tube
Detector resolution: 8.53 pixels mm^{-1}
rotating crystal scans
Absorption correction: multi-scan (SADABS; Bruker, 2018)
$T_{min} = 0.741$, $T_{max} = 1.000$
13278 measured reflections
1970 independent reflections
1674 reflections with $I > 2\sigma(I)$
$R_{int} = 0.057$
$\theta_{max} = 26.4$°, $\theta_{min} = 1.7$°
$h = -6 \rightarrow 6$
$k = -9 \rightarrow 9$
$l = -15 \rightarrow 15$

Refinement

Refinement on F^2
Least-squares matrix: full
$R[F^2 > 2\sigma(F^2)] = 0.042$
$wR(F^2) = 0.115$
$S = 1.05$
1970 reflections
167 parameters
7 restraints
Primary atom site location: structure-invariant direct methods
Hydrogen site location: mixed
H atoms treated by a mixture of independent and constrained refinement
$w = 1/[\sigma^2(F_o^2) + (0.0493P)^2 + 0.2673P]$ where $P = (F_o^2 + 2F_c^2)/3$
$(\Delta/\sigma)_{max} < 0.001$
$\Delta\rho_{max} = 0.30$ e Å^{-3}
$\Delta\rho_{min} = -0.28$ e Å^{-3}

Special details

Geometry. All esds (except the esd in the dihedral angle between two l.s. planes) are estimated using the full covariance matrix. The cell esds are taken into account individually in the estimation of esds in distances, angles and torsion angles; correlations between esds in cell parameters are only used when they are defined by crystal symmetry. An approximate (isotropic) treatment of cell esds is used for estimating esds involving l.s. planes.

Fractional atomic coordinates and isotropic or equivalent isotropic displacement parameters (Å²)

	x	*y*	*z*	U_{iso}*/U_{eq}	Occ. (<1)
O1	−0.1287 (2)	0.2405 (2)	0.53846 (12)	0.0499 (4)	
N1	0.2795 (3)	0.2386 (2)	0.57014 (12)	0.0330 (4)	
C1	0.1041 (3)	0.2499 (2)	0.50193 (15)	0.0319 (4)	
C2	0.2125 (3)	0.2733 (2)	0.37796 (14)	0.0291 (4)	
C3	0.0703 (4)	0.2069 (2)	0.30678 (16)	0.0346 (4)	
C4	0.1559 (4)	0.2293 (3)	0.19123 (17)	0.0413 (5)	
C5	0.3815 (4)	0.3210 (3)	0.14528 (17)	0.0421 (5)	
C6	0.5229 (4)	0.3882 (3)	0.21505 (17)	0.0400 (5)	
C7	0.4407 (3)	0.3640 (2)	0.33099 (16)	0.0347 (4)	
C8	0.2173 (3)	0.2173 (2)	0.68901 (14)	0.0298 (4)	
C9	0.3833 (4)	0.1279 (3)	0.75218 (15)	0.0378 (4)	
C11	−0.0008 (4)	0.2800 (3)	0.75581 (15)	0.0375 (4)	
C10A	0.2963 (7)	0.1217 (7)	0.8636 (3)	0.0427 (2)	0.7018 (16)
S1A	−0.00570 (18)	0.23139 (17)	0.89493 (6)	0.0427 (2)	0.7018 (16)
C10B	−0.0046 (17)	0.2407 (18)	0.8655 (5)	0.0427 (2)	0.2982 (16)
H10B	−0.140418	0.272729	0.923742	0.051*	0.2982 (16)
S1B	0.2743 (4)	0.1213 (4)	0.89031 (14)	0.0427 (2)	0.2982 (16)
H1	0.462 (2)	0.235 (3)	0.5360 (17)	0.048 (6)*	
H9	0.543 (4)	0.080 (3)	0.7220 (19)	0.046 (6)*	
H11	−0.139 (4)	0.344 (3)	0.7308 (18)	0.045 (6)*	
H10A	0.385 (6)	0.067 (4)	0.935 (3)	0.051 (9)*	0.7018 (16)
H3	−0.086 (4)	0.145 (3)	0.3390 (17)	0.038 (5)*	
H7	0.540 (4)	0.411 (3)	0.3815 (19)	0.046 (6)*	
H6	0.674 (5)	0.449 (3)	0.1854 (19)	0.051 (6)*	
H4	0.048 (5)	0.181 (3)	0.144 (2)	0.054 (6)*	
H5	0.437 (5)	0.344 (3)	0.065 (2)	0.057 (7)*	

Atomic displacement parameters (Å²)

	U^{11}	U^{22}	U^{33}	U^{12}	U^{13}	U^{23}
O1	0.0274 (7)	0.0870 (12)	0.0351 (8)	−0.0041 (7)	−0.0060 (6)	−0.0054 (7)
N1	0.0261 (7)	0.0453 (9)	0.0279 (8)	−0.0009 (6)	−0.0058 (6)	−0.0043 (6)
C1	0.0275 (8)	0.0363 (9)	0.0326 (9)	−0.0023 (7)	−0.0071 (7)	−0.0041 (7)
C2	0.0279 (8)	0.0300 (8)	0.0303 (9)	0.0032 (6)	−0.0083 (7)	−0.0037 (7)
C3	0.0324 (9)	0.0362 (10)	0.0373 (10)	−0.0023 (7)	−0.0100 (8)	−0.0066 (8)
C4	0.0467 (11)	0.0454 (11)	0.0368 (10)	0.0036 (9)	−0.0162 (9)	−0.0130 (8)
C5	0.0481 (11)	0.0485 (12)	0.0284 (10)	0.0072 (9)	−0.0052 (8)	−0.0048 (8)
C6	0.0367 (10)	0.0402 (11)	0.0401 (11)	−0.0021 (8)	−0.0024 (8)	0.0006 (8)
C7	0.0336 (9)	0.0361 (10)	0.0359 (10)	−0.0026 (7)	−0.0098 (7)	−0.0038 (8)

C8	0.0292 (8)	0.0314 (9)	0.0295 (9)	−0.0064 (7)	−0.0067 (7)	−0.0035 (7)
C9	0.0326 (9)	0.0426 (11)	0.0395 (11)	0.0002 (8)	−0.0113 (8)	−0.0019 (8)
C11	0.0338 (9)	0.0445 (11)	0.0341 (10)	0.0010 (8)	−0.0059 (8)	−0.0059 (8)
C10A	0.0430 (4)	0.0572 (4)	0.0262 (5)	−0.0037 (3)	−0.0037 (3)	−0.0024 (4)
S1A	0.0430 (4)	0.0572 (4)	0.0262 (5)	−0.0037 (3)	−0.0037 (3)	−0.0024 (4)
C10B	0.0430 (4)	0.0572 (4)	0.0262 (5)	−0.0037 (3)	−0.0037 (3)	−0.0024 (4)
S1B	0.0430 (4)	0.0572 (4)	0.0262 (5)	−0.0037 (3)	−0.0037 (3)	−0.0024 (4)

Geometric parameters (Å, º)

O1—C1	1.224 (2)	C6—H6	0.92 (2)
N1—C1	1.358 (2)	C7—H7	0.98 (2)
N1—C8	1.408 (2)	C8—C11	1.380 (3)
N1—H1	0.974 (10)	C8—C9	1.399 (2)
C1—C2	1.494 (2)	C9—C10A	1.336 (4)
C2—C7	1.392 (2)	C9—S1B	1.658 (2)
C2—C3	1.394 (2)	C9—H9	0.93 (2)
C3—C4	1.380 (3)	C11—C10B	1.331 (5)
C3—H3	0.95 (2)	C11—S1A	1.6869 (18)
C4—C5	1.383 (3)	C11—H11	0.95 (2)
C4—H4	0.98 (2)	C10A—S1A	1.779 (3)
C5—C6	1.380 (3)	C10A—H10A	1.11 (3)
C5—H5	0.96 (3)	C10B—S1B	1.777 (4)
C6—C7	1.383 (3)	C10B—H10B	0.9500
C1—N1—C8	124.73 (15)	C2—C7—H7	118.9 (13)
C1—N1—H1	118.8 (13)	C11—C8—C9	112.69 (17)
C8—N1—H1	116.3 (13)	C11—C8—N1	126.24 (16)
O1—C1—N1	122.79 (17)	C9—C8—N1	121.07 (16)
O1—C1—C2	121.37 (15)	C10A—C9—C8	113.2 (2)
N1—C1—C2	115.84 (15)	C8—C9—S1B	112.93 (16)
C7—C2—C3	119.17 (17)	C10A—C9—H9	121.6 (14)
C7—C2—C1	123.18 (15)	C8—C9—H9	125.1 (14)
C3—C2—C1	117.60 (16)	S1B—C9—H9	121.9 (14)
C4—C3—C2	120.38 (18)	C10B—C11—C8	112.4 (3)
C4—C3—H3	120.6 (12)	C8—C11—S1A	112.60 (14)
C2—C3—H3	119.0 (12)	C10B—C11—H11	120.7 (13)
C3—C4—C5	120.04 (18)	C8—C11—H11	126.9 (13)
C3—C4—H4	117.5 (14)	S1A—C11—H11	120.5 (13)
C5—C4—H4	122.5 (14)	C9—C10A—S1A	111.1 (3)
C6—C5—C4	119.99 (19)	C9—C10A—H10A	130.9 (17)
C6—C5—H5	119.2 (15)	S1A—C10A—H10A	117.9 (17)
C4—C5—H5	120.8 (15)	C11—S1A—C10A	90.34 (16)
C5—C6—C7	120.37 (19)	C11—C10B—S1B	112.0 (4)
C5—C6—H6	120.8 (15)	C11—C10B—H10B	124.0
C7—C6—H6	118.8 (15)	S1B—C10B—H10B	124.0
C6—C7—C2	120.04 (17)	C9—S1B—C10B	89.9 (3)
C6—C7—H7	121.1 (13)		

C8—N1—C1—O1	−0.8 (3)	C1—N1—C8—C9	149.82 (18)
C8—N1—C1—C2	179.66 (15)	C11—C8—C9—C10A	0.0 (3)
O1—C1—C2—C7	148.68 (19)	N1—C8—C9—C10A	179.2 (3)
N1—C1—C2—C7	−31.8 (2)	C11—C8—C9—S1B	−0.1 (2)
O1—C1—C2—C3	−28.5 (3)	N1—C8—C9—S1B	179.08 (17)
N1—C1—C2—C3	151.03 (17)	C9—C8—C11—C10B	−0.2 (7)
C7—C2—C3—C4	0.6 (3)	N1—C8—C11—C10B	−179.3 (7)
C1—C2—C3—C4	177.89 (17)	C9—C8—C11—S1A	0.1 (2)
C2—C3—C4—C5	−1.2 (3)	N1—C8—C11—S1A	−179.05 (14)
C3—C4—C5—C6	0.8 (3)	C8—C9—C10A—S1A	−0.1 (4)
C4—C5—C6—C7	0.2 (3)	C8—C11—S1A—C10A	−0.1 (2)
C5—C6—C7—C2	−0.8 (3)	C9—C10A—S1A—C11	0.2 (4)
C3—C2—C7—C6	0.4 (3)	C8—C11—C10B—S1B	0.4 (11)
C1—C2—C7—C6	−176.73 (17)	C8—C9—S1B—C10B	0.3 (6)
C1—N1—C8—C11	−31.1 (3)	C11—C10B—S1B—C9	−0.4 (10)

Hydrogen-bond geometry (Å, º)

D—H···*A*	*D*—H	H···*A*	*D*···*A*	*D*—H···*A*
N1—H1···O1^{i}	0.97 (1)	2.17 (1)	3.078 (2)	154 (2)

Symmetry code: (i) *x*+1, *y*, *z*.

N-(Furan-3-yl)benzamide (FAP)

Crystal data

$C_{11}H_9NO_2$
M_r = 187.19
Triclinic, $P\overline{1}$
a = 9.0111 (3) Å
b = 9.8038 (3) Å
c = 11.3362 (4) Å
α = 109.081 (3)°
β = 99.580 (3)°
γ = 90.499 (3)°
V = 931.11 (6) Å^3

Z = 4
$F(000)$ = 392
D_x = 1.335 Mg m^{-3}
Mo $K\alpha$ radiation, λ = 0.71073 Å
Cell parameters from 9231 reflections
θ = 2.2–27.7°
μ = 0.09 mm^{-1}
T = 172 K
Parallelpiped, colourless
0.28 × 0.24 × 0.16 mm

Data collection

Rigaku OD SuperNova Dual source diffractometer with an Atlas detector
Radiation source: micro-focus sealed X-ray tube, SuperNova (Mo) X-ray Source
Mirror monochromator
Detector resolution: 5.1937 pixels mm^{-1}
ω scans
Absorption correction: gaussian (CrysAlis PRO; Rigaku OD, 2020)

T_{min} = 0.589, T_{max} = 1.000
21889 measured reflections
4363 independent reflections
3580 reflections with $I > 2\sigma(I)$
R_{int} = 0.027
θ_{max} = 27.7°, θ_{min} = 2.2°
h = −11→11
k = −12→12
l = −14→14

Refinement

Refinement on F^2
Least-squares matrix: full
$R[F^2 > 2\sigma(F^2)] = 0.047$
$wR(F^2) = 0.125$
$S = 1.09$
4363 reflections
325 parameters
2 restraints

Primary atom site location: structure-invariant direct methods
Hydrogen site location: difference Fourier map
All H-atom parameters refined
$w = 1/[\sigma^2(F_o^2) + (0.0358P)^2 + 0.5819P]$ where $P = (F_o^2 + 2F_c^2)/3$
$(\Delta/\sigma)_{max} < 0.001$
$\Delta\rho_{max} = 0.43$ e Å^{-3}
$\Delta\rho_{min} = -0.21$ e Å^{-3}

Special details

Geometry. All esds (except the esd in the dihedral angle between two l.s. planes) are estimated using the full covariance matrix. The cell esds are taken into account individually in the estimation of esds in distances, angles and torsion angles; correlations between esds in cell parameters are only used when they are defined by crystal symmetry. An approximate (isotropic) treatment of cell esds is used for estimating esds involving l.s. planes.

Fractional atomic coordinates and isotropic or equivalent isotropic displacement parameters (Å^2)

	x	*y*	*z*	U_{iso}*/U_{eq}
O2B	0.31100 (15)	0.92606 (15)	0.14475 (12)	0.0433 (3)
O1B	0.19284 (17)	1.16489 (13)	0.48727 (12)	0.0445 (3)
O1A	0.26070 (16)	0.65821 (13)	0.46386 (12)	0.0436 (3)
N1B	0.28195 (16)	0.94517 (14)	0.46251 (13)	0.0304 (3)
O2A	−0.02588 (17)	0.40167 (16)	0.13362 (13)	0.0499 (4)
N1A	0.17171 (16)	0.43463 (15)	0.44552 (14)	0.0336 (3)
C8B	0.30352 (18)	0.91697 (16)	0.33742 (15)	0.0295 (3)
C2B	0.20979 (18)	1.07866 (16)	0.66239 (15)	0.0304 (3)
C1A	0.25737 (19)	0.55835 (17)	0.50642 (16)	0.0319 (4)
C2A	0.35395 (19)	0.56779 (17)	0.63096 (16)	0.0323 (4)
C1B	0.22725 (19)	1.06763 (16)	0.53109 (16)	0.0310 (3)
C8A	0.08253 (19)	0.40288 (18)	0.32530 (16)	0.0342 (4)
C11B	0.2766 (2)	0.9986 (2)	0.26170 (17)	0.0362 (4)
C9A	−0.0113 (2)	0.2719 (2)	0.26277 (18)	0.0382 (4)
C9B	0.3584 (2)	0.78542 (19)	0.26439 (18)	0.0377 (4)
C7A	0.3157 (2)	0.49179 (19)	0.70655 (18)	0.0380 (4)
C7B	0.3024 (2)	1.0114 (2)	0.73419 (17)	0.0380 (4)
C3B	0.0988 (2)	1.1635 (2)	0.71490 (18)	0.0389 (4)
C3A	0.4849 (2)	0.65950 (19)	0.67193 (18)	0.0390 (4)
C10A	−0.0726 (2)	0.2780 (2)	0.14880 (19)	0.0431 (4)
C11A	0.0708 (2)	0.4795 (2)	0.24367 (18)	0.0403 (4)
C10B	0.3605 (2)	0.7969 (2)	0.15032 (19)	0.0439 (4)
C6A	0.4077 (2)	0.5072 (2)	0.82095 (19)	0.0443 (5)
C6B	0.2833 (2)	1.0287 (2)	0.85718 (19)	0.0462 (5)
C5B	0.1717 (2)	1.1114 (2)	0.90777 (18)	0.0479 (5)
C5A	0.5375 (2)	0.5977 (2)	0.86116 (18)	0.0453 (5)
C4B	0.0796 (2)	1.1792 (2)	0.83709 (19)	0.0462 (5)
C4A	0.5761 (2)	0.6735 (2)	0.78663 (19)	0.0456 (5)
H7B	0.382 (2)	0.952 (2)	0.6991 (19)	0.044 (5)*
H7A	0.222 (2)	0.426 (2)	0.676 (2)	0.049 (6)*

H3A	0.514 (2)	0.716 (2)	0.616 (2)	0.052 (6)*
H3B	0.038 (2)	1.214 (2)	0.666 (2)	0.050 (6)*
H4B	0.003 (3)	1.236 (2)	0.873 (2)	0.055 (6)*
H5B	0.155 (3)	1.123 (2)	0.993 (2)	0.056 (6)*
H5A	0.602 (3)	0.608 (2)	0.940 (2)	0.060 (7)*
H6A	0.377 (3)	0.451 (3)	0.871 (2)	0.064 (7)*
H6B	0.350 (3)	0.980 (3)	0.904 (2)	0.062 (7)*
H4A	0.667 (3)	0.738 (3)	0.815 (2)	0.059 (7)*
H1A	0.183 (2)	0.357 (2)	0.4812 (19)	0.050 (6)*
H11B	0.234 (2)	1.088 (2)	0.2707 (18)	0.038 (5)*
H11A	0.118 (2)	0.567 (2)	0.2491 (18)	0.038 (5)*
H9B	0.390 (2)	0.710 (2)	0.2929 (19)	0.043 (5)*
H9A	−0.027 (2)	0.200 (2)	0.295 (2)	0.053 (6)*
H10B	0.388 (3)	0.736 (2)	0.073 (2)	0.057 (6)*
H10A	−0.139 (3)	0.217 (3)	0.083 (2)	0.069 (7)*
H1B	0.287 (2)	0.8661 (19)	0.4924 (19)	0.047 (6)*

Atomic displacement parameters (Å²)

	U^{11}	U^{22}	U^{33}	U^{12}	U^{13}	U^{23}
O2B	0.0514 (8)	0.0488 (8)	0.0326 (7)	0.0048 (6)	0.0119 (6)	0.0152 (6)
O1B	0.0734 (10)	0.0246 (6)	0.0412 (7)	0.0117 (6)	0.0174 (7)	0.0151 (5)
O1A	0.0629 (9)	0.0266 (6)	0.0442 (7)	−0.0006 (6)	0.0038 (6)	0.0184 (5)
N1B	0.0407 (8)	0.0223 (6)	0.0317 (7)	0.0040 (5)	0.0108 (6)	0.0117 (6)
O2A	0.0573 (9)	0.0547 (9)	0.0375 (7)	0.0109 (7)	0.0053 (6)	0.0165 (6)
N1A	0.0394 (8)	0.0257 (7)	0.0375 (8)	0.0034 (6)	0.0056 (6)	0.0134 (6)
C8B	0.0315 (8)	0.0247 (7)	0.0324 (8)	−0.0007 (6)	0.0073 (6)	0.0090 (6)
C2B	0.0346 (8)	0.0228 (7)	0.0317 (8)	−0.0043 (6)	0.0063 (7)	0.0062 (6)
C1A	0.0394 (9)	0.0235 (7)	0.0355 (9)	0.0053 (6)	0.0113 (7)	0.0111 (7)
C2A	0.0386 (9)	0.0248 (8)	0.0347 (9)	0.0075 (6)	0.0123 (7)	0.0086 (7)
C1B	0.0375 (9)	0.0222 (7)	0.0337 (8)	−0.0001 (6)	0.0081 (7)	0.0089 (6)
C8A	0.0346 (9)	0.0329 (8)	0.0364 (9)	0.0107 (7)	0.0092 (7)	0.0117 (7)
C11B	0.0432 (10)	0.0349 (9)	0.0333 (9)	0.0041 (7)	0.0107 (7)	0.0129 (7)
C9A	0.0399 (10)	0.0329 (9)	0.0405 (10)	0.0035 (7)	0.0088 (8)	0.0097 (8)
C9B	0.0437 (10)	0.0306 (9)	0.0399 (10)	0.0052 (7)	0.0144 (8)	0.0097 (8)
C7A	0.0440 (10)	0.0341 (9)	0.0388 (10)	0.0061 (8)	0.0122 (8)	0.0136 (8)
C7B	0.0360 (9)	0.0411 (10)	0.0360 (9)	0.0005 (8)	0.0060 (7)	0.0118 (8)
C3B	0.0423 (10)	0.0344 (9)	0.0386 (10)	0.0026 (7)	0.0105 (8)	0.0086 (8)
C3A	0.0434 (10)	0.0337 (9)	0.0408 (10)	0.0015 (7)	0.0093 (8)	0.0128 (8)
C10A	0.0422 (11)	0.0416 (10)	0.0379 (10)	0.0026 (8)	0.0022 (8)	0.0055 (8)
C11A	0.0457 (11)	0.0382 (10)	0.0383 (10)	0.0090 (8)	0.0073 (8)	0.0146 (8)
C10B	0.0507 (11)	0.0413 (10)	0.0377 (10)	0.0044 (8)	0.0157 (8)	0.0066 (8)
C6A	0.0573 (12)	0.0440 (10)	0.0405 (10)	0.0131 (9)	0.0185 (9)	0.0210 (9)
C6B	0.0438 (11)	0.0592 (13)	0.0353 (10)	−0.0038 (9)	0.0002 (8)	0.0189 (9)
C5B	0.0491 (11)	0.0599 (13)	0.0285 (9)	−0.0131 (9)	0.0079 (8)	0.0062 (9)
C5A	0.0502 (12)	0.0506 (11)	0.0315 (10)	0.0145 (9)	0.0036 (8)	0.0104 (8)
C4B	0.0470 (11)	0.0486 (11)	0.0384 (10)	0.0013 (9)	0.0164 (9)	0.0042 (9)
C4A	0.0420 (11)	0.0464 (11)	0.0442 (11)	0.0001 (9)	0.0036 (8)	0.0117 (9)

Geometric parameters (Å, º)

O2B—C10B	1.363 (2)	C9A—H9A	0.92 (2)
O2B—C11B	1.372 (2)	C9B—C10B	1.337 (3)
O1B—C1B	1.2312 (19)	C9B—H9B	0.93 (2)
O1A—C1A	1.2269 (19)	C7A—C6A	1.380 (3)
N1B—C1B	1.348 (2)	C7A—H7A	1.00 (2)
N1B—C8B	1.400 (2)	C7B—C6B	1.388 (3)
N1B—H1B	0.941 (15)	C7B—H7B	0.98 (2)
O2A—C10A	1.352 (2)	C3B—C4B	1.383 (3)
O2A—C11A	1.379 (2)	C3B—H3B	0.96 (2)
N1A—C1A	1.343 (2)	C3A—C4A	1.382 (3)
N1A—C8A	1.398 (2)	C3A—H3A	1.02 (2)
N1A—H1A	0.970 (15)	C10A—H10A	0.91 (3)
C8B—C11B	1.349 (2)	C11A—H11A	0.93 (2)
C8B—C9B	1.429 (2)	C10B—H10B	0.96 (2)
C2B—C7B	1.389 (2)	C6A—C5A	1.380 (3)
C2B—C3B	1.391 (2)	C6A—H6A	0.98 (2)
C2B—C1B	1.492 (2)	C6B—C5B	1.378 (3)
C1A—C2A	1.504 (2)	C6B—H6B	0.96 (2)
C2A—C7A	1.386 (2)	C5B—C4B	1.382 (3)
C2A—C3A	1.394 (2)	C5B—H5B	0.97 (2)
C8A—C11A	1.362 (3)	C5A—C4A	1.375 (3)
C8A—C9A	1.433 (2)	C5A—H5A	0.96 (2)
C11B—H11B	0.95 (2)	C4B—H4B	0.95 (2)
C9A—C10A	1.339 (3)	C4A—H4A	0.97 (2)
C10B—O2B—C11B	106.20 (14)	C2A—C7A—H7A	118.8 (12)
C1B—N1B—C8B	123.73 (14)	C6B—C7B—C2B	119.94 (18)
C1B—N1B—H1B	118.6 (13)	C6B—C7B—H7B	119.4 (12)
C8B—N1B—H1B	116.3 (13)	C2B—C7B—H7B	120.7 (12)
C10A—O2A—C11A	107.18 (15)	C4B—C3B—C2B	120.27 (19)
C1A—N1A—C8A	124.03 (14)	C4B—C3B—H3B	120.8 (13)
C1A—N1A—H1A	118.0 (13)	C2B—C3B—H3B	118.9 (13)
C8A—N1A—H1A	117.4 (13)	C4A—C3A—C2A	120.13 (18)
C11B—C8B—N1B	129.87 (15)	C4A—C3A—H3A	120.1 (12)
C11B—C8B—C9B	106.75 (15)	C2A—C3A—H3A	119.7 (12)
N1B—C8B—C9B	123.37 (15)	C9A—C10A—O2A	111.37 (17)
C7B—C2B—C3B	119.47 (16)	C9A—C10A—H10A	132.5 (16)
C7B—C2B—C1B	122.54 (16)	O2A—C10A—H10A	116.1 (16)
C3B—C2B—C1B	117.97 (16)	C8A—C11A—O2A	108.58 (17)
O1A—C1A—N1A	123.10 (16)	C8A—C11A—H11A	132.0 (12)
O1A—C1A—C2A	120.84 (15)	O2A—C11A—H11A	119.3 (12)
N1A—C1A—C2A	116.04 (14)	C9B—C10B—O2B	111.16 (17)
C7A—C2A—C3A	119.44 (17)	C9B—C10B—H10B	135.3 (14)
C7A—C2A—C1A	122.55 (16)	O2B—C10B—H10B	113.5 (14)
C3A—C2A—C1A	118.00 (15)	C5A—C6A—C7A	120.76 (18)
O1B—C1B—N1B	121.65 (15)	C5A—C6A—H6A	122.4 (14)

O1B—C1B—C2B	121.83 (15)	C7A—C6A—H6A	116.9 (15)
N1B—C1B—C2B	116.52 (14)	C5B—C6B—C7B	120.2 (2)
C11A—C8A—N1A	129.48 (17)	C5B—C6B—H6B	122.6 (14)
C11A—C8A—C9A	107.04 (17)	C7B—C6B—H6B	117.3 (14)
N1A—C8A—C9A	123.42 (16)	C6B—C5B—C4B	120.23 (18)
C8B—C11B—O2B	109.84 (16)	C6B—C5B—H5B	121.3 (14)
C8B—C11B—H11B	133.9 (12)	C4B—C5B—H5B	118.5 (14)
O2B—C11B—H11B	116.1 (12)	C4A—C5A—C6A	119.81 (19)
C10A—C9A—C8A	105.83 (17)	C4A—C5A—H5A	119.2 (14)
C10A—C9A—H9A	127.4 (14)	C6A—C5A—H5A	121.0 (14)
C8A—C9A—H9A	126.7 (14)	C5B—C4B—C3B	119.93 (19)
C10B—C9B—C8B	106.05 (17)	C5B—C4B—H4B	119.3 (14)
C10B—C9B—H9B	127.8 (13)	C3B—C4B—H4B	120.7 (14)
C8B—C9B—H9B	126.1 (13)	C5A—C4A—C3A	120.15 (19)
C6A—C7A—C2A	119.72 (18)	C5A—C4A—H4A	120.2 (14)
C6A—C7A—H7A	121.4 (12)	C3A—C4A—H4A	119.6 (14)

C1B—N1B—C8B—C11B	−0.2 (3)	C3A—C2A—C7A—C6A	−0.3 (3)
C1B—N1B—C8B—C9B	−178.55 (16)	C1A—C2A—C7A—C6A	−178.81 (16)
C8A—N1A—C1A—O1A	3.0 (3)	C3B—C2B—C7B—C6B	0.2 (3)
C8A—N1A—C1A—C2A	−175.73 (15)	C1B—C2B—C7B—C6B	178.28 (16)
O1A—C1A—C2A—C7A	153.91 (17)	C7B—C2B—C3B—C4B	−0.8 (3)
N1A—C1A—C2A—C7A	−27.4 (2)	C1B—C2B—C3B—C4B	−178.96 (16)
O1A—C1A—C2A—C3A	−24.6 (2)	C7A—C2A—C3A—C4A	0.4 (3)
N1A—C1A—C2A—C3A	154.10 (16)	C1A—C2A—C3A—C4A	179.01 (17)
C8B—N1B—C1B—O1B	−0.4 (3)	C8A—C9A—C10A—O2A	−0.1 (2)
C8B—N1B—C1B—C2B	179.22 (14)	C11A—O2A—C10A—C9A	0.0 (2)
C7B—C2B—C1B—O1B	−150.48 (18)	N1A—C8A—C11A—O2A	176.97 (16)
C3B—C2B—C1B—O1B	27.6 (2)	C9A—C8A—C11A—O2A	−0.1 (2)
C7B—C2B—C1B—N1B	29.9 (2)	C10A—O2A—C11A—C8A	0.0 (2)
C3B—C2B—C1B—N1B	−152.06 (16)	C8B—C9B—C10B—O2B	0.0 (2)
C1A—N1A—C8A—C11A	5.0 (3)	C11B—O2B—C10B—C9B	0.1 (2)
C1A—N1A—C8A—C9A	−178.37 (16)	C2A—C7A—C6A—C5A	0.1 (3)
N1B—C8B—C11B—O2B	−178.43 (16)	C2B—C7B—C6B—C5B	0.6 (3)
C9B—C8B—C11B—O2B	0.2 (2)	C7B—C6B—C5B—C4B	−0.9 (3)
C10B—O2B—C11B—C8B	−0.2 (2)	C7A—C6A—C5A—C4A	−0.1 (3)
C11A—C8A—C9A—C10A	0.1 (2)	C6B—C5B—C4B—C3B	0.3 (3)
N1A—C8A—C9A—C10A	−177.17 (16)	C2B—C3B—C4B—C5B	0.6 (3)
C11B—C8B—C9B—C10B	−0.1 (2)	C6A—C5A—C4A—C3A	0.2 (3)
N1B—C8B—C9B—C10B	178.60 (16)	C2A—C3A—C4A—C5A	−0.4 (3)

Hydrogen-bond geometry (Å, º)

D—H···*A*	*D*—H	H···*A*	*D*···*A*	*D*—H···*A*
N1*B*—H1*B*···O1*A*	0.94 (2)	1.96 (2)	2.8234 (17)	151 (2)
N1*A*—H1*A*···O1*B*^{i}	0.97 (2)	1.91 (2)	2.8374 (18)	159 (2)

Symmetry code: (i) *x*, *y*−1, *z*.